British Journal of Pharmacology (2008) 155, 34–43

0007–1188/08 $30.00
www.brjpharmacol.org

RESEARCH PAPER

Low concentrations of tetrodotoxin interact with tetrodotoxin-resistant voltage-gated sodium channels

CE Farmer[1,3], KJ Smith[1,4] and RJ Docherty[2]

[1]*King's College London, Department of Clinical Neurosciences, London, UK and* [2]*King's College London, Neurorestoration Group, Wolfson Centre for Age-Related Diseases, London, UK*

Background and purpose: Tetrodotoxin (TTX) is used to distinguish between two classes of voltage-gated sodium channel (VGSC)—TTX sensitive (TTXS) and TTX resistant (TTXR). The resistance of TTXR VGSCs is thought to result from a low binding affinity of TTX, although at high TTX concentrations channel block does occur. Here, we show that, at concentrations below those which produce block, TTX can bind to TTXR VGSCs.
Experimental approach: Whole-cell voltage clamp recordings were made from dissociated rat dorsal root ganglion neurones that expressed both TTXS and TTXR sodium currents. Voltage-gated calcium currents were blocked by 10 μM extracellular lanthanum chloride. TTXS, but not TTXR, current was suppressed by using a holding potential of −50 mV, and the effect of TTX on the isolated TTXR current was explored.
Key results: Extracellular application of 0.5 μM TTX produced a 40% increase in TTXR current amplitude, a negative shift in the voltage-dependence of current activation (approximately −8 mV) and inactivation (approximately −10 mV) and increased rates of current activation and inactivation. The effect of TTX on current amplitude was dose-dependent ($EC_{50} = 364$ nM). Removal of lanthanum prevented the effect of TTX on TTXR current amplitude, whereas reducing extracellular calcium did not.
Conclusions and implications: The findings are consistent with an interpretation that TTX relieves a tonic block of the TTXR VGSC by lanthanum. We conclude that TTX binds to the TTXR VGSC at low concentrations, without blocking it. This appears to be the first demonstration of a clear distinction between binding affinity and blocking potency of a channel-blocking agent.
British Journal of Pharmacology (2008) **155,** 34–43; doi:10.1038/bjp.2008.235; published online 16 June 2008

Keywords: voltage-gated sodium channel; sodium current; tetrodotoxin; tetrodotoxin-resistant

Abbreviations: DRG, dorsal root ganglion; TTX, tetrodotoxin; TTXR, TTX-resistant; TTXS, TTX-sensitive; VGSC, voltage-gated sodium channel

Introduction

The discovery of a selective blocking action of tetrodotoxin (TTX) (Narahashi, 1974) on voltage-gated sodium channels (VGSCs) has been of immeasurable value for investigations of the properties and physiological roles of VGSCs, as well as their pharmacology. TTX is a convenient pharmacological tool that can be used to distinguish two classes of VGSCs—those that are blocked by submicromolar concentrations of the toxin (TTX-sensitive (TTXS)) and those where the blocking action requires much higher concentrations (TTX-resistant (TTXR)). This distinction has proved especially useful in studies of sensory neurones of the dorsal root ganglion (DRG) where all of the neurones express TTXS currents, but only about half the population of small neurones express an additional TTXR current (Kostyuk *et al.*, 1981; Roy and Narahashi, 1992; Elliott and Elliott, 1993). The TTXR-expressing neurones are a subset of the C-fibre and Aδ-fibre populations including capsaicin-sensitive nociceptors (McLean *et al.*, 1988; Pearce and Duchen, 1994; Arbuckle and Docherty, 1995) and high-threshold mechanoreceptors (Akopian *et al.*, 1999).

The TTXR currents can be further subdivided into at least three subtypes, described as TTXR1, TTXR2 and TTXR3 (Rush *et al.*, 1998), using voltage-clamp protocols that exploit their distinct voltage-dependent properties. These currents probably correspond to molecularly identified forms of TTXR channels, namely $Na_V1.8$ (Akopian *et al.*, 1996; Sangameswaran *et al.*, 1996) and $Na_V1.9$

Correspondence: Dr CE Farmer, Department of Molecular Neuroscience, Institute of Neurology, University College London, Queen Square, London WC1N 3BG, UK.
E-mail: c.farmer@ion.ucl.ac.uk
[3]Current address: Department of Molecular Neuroscience, Institute of Neurology, University College London, London, UK.
[4]Current address: Department of Neuroinflammation, Institute of Neurology, University College London, London, UK.
Received 19 December 2007; revised 7 March 2008; accepted 25 April 2008; published online 16 June 2008

(Dib-Hajj *et al*., 2002), which give rise to a slow transient current and a low-threshold persistent current, respectively, and $Na_V1.5$, which is relatively rare in adult neurones and gives rise to a fast transient current (Renganathan *et al*., 2002). A recent analysis of the evidence suggests that the physiological role of the $Na_V1.8$ TTXR currents is to protect sensory neuronal somata from depolarization-induced block of action potential firing, whereas $Na_V1.9$ channels may be of more importance in generating spontaneous firing or sustaining bursts of firing nearer the resting potential (Rush *et al*., 2007).

As $Na_V1.8$ and $Na_V1.9$ are expressed predominantly in peripheral sensory neurones, including nociceptive neurones, blockers of these VGSCs would be expected to have analgesic properties (Lai *et al*., 2004) and therefore the channels are considered important targets for the discovery of novel analgesic drugs. The EC50s for the block of $Na_V1.8$ and $Na_V1.9$ by TTX are estimated to be about 60 μM (Akopian *et al*., 1996) and 40 μM (Cummins *et al*., 1999), respectively, suggesting that the binding site for TTX, usually referred to as site 1 (Cestèle and Catterall, 2000), is of fairly low affinity in the TTXR subtypes. Here, we describe experiments that show that this assumption may not be true. Thus, although low concentrations of TTX do not block TTXR channels, they do nonetheless affect their behaviour in such a way as to suggest that the toxin binds to the TTXR channels with submicromolar affinity.

Materials and methods

Animals

All animal procedures complied with the UK Animals (Scientific Procedures) Act 1986. Rats (Harlan, UK) were maintained in a humidity- and temperature-controlled environment with free access to food and water. Animals (200–400 g of either sex) were killed in a chamber filled with a slowly rising concentration of CO_2.

Cell culture

Dorsal root ganglion neurones were isolated from adult Lewis ($n=7$) or Sprague–Dawley rats ($n=3$). The lumbar DRGs were dissected, trimmed free of processes, placed in a Petri dish containing Dulbecco's modified Eagle's medium F12 Ham's solution (Sigma, Poole, UK) supplemented with 0.125% type III collagenase (Worthington Biochemical Corporation, Lakewood, NJ, USA) and transferred to an incubator containing a 5% CO_2/air atmosphere at 37 °C for 3 h. The partially digested ganglia were washed with fresh Dulbecco's modified Eagle's medium F12 Ham's medium, and then the cells were dissociated by trituration in the same medium supplemented with 10% foetal bovine serum (Gibco, Invitrogen, Paisley, UK), 0.1 mg mL^{-1} streptomycin (Sigma) and 100 U mL^{-1} penicillin (Sigma). The dissociated ganglia were centrifuged at approximately 1000 × *g* for 5 min and the cell pellet was resuspended in a medium that was identical to the trituration medium. Cells were plated on to polyornithine-coated glass coverslips for electrophysiology and stored in the incubator for up to 48 h before use. Cells were replated 3–9 h before recording to minimize the outgrowth of processes.

Electrophysiology

Whole-cell voltage clamp electrophysiological recordings were made using electrodes (resistance 2–5 MOhm) filled with a solution of the following composition (in mM): NaCl, 10; CsCl, 110; $MgCl_2$, 1; $CaCl_2$, 0.1; EGTA, 10; HEPES, 5; pH = 7.4 (adjusted with NaOH). The superfusing extracellular solution was of the following composition (in mM): NaCl, 39; choline Cl, 91; $MgCl_2$, 1; CsCl, 3; $CaCl_2$, 1; HEPES, 5; glucose, 11, $LaCl_3$, 0.01; pH = 7.4 (adjusted with NaOH). The solutions were designed to isolate voltage-gated sodium currents; CsCl was included in place of KCl both intra- and extracellularly to prevent voltage-gated potassium currents, and $LaCl_3$ was included in the extracellular buffer to block voltage-gated calcium currents. In the extracellular solution, 70% of the NaCl was replaced by choline chloride. This low sodium concentration was required to reduce the size of the sodium currents so that they could be controlled effectively by the voltage clamp. In other published data on TTXR sodium currents fluoride is sometimes included in the

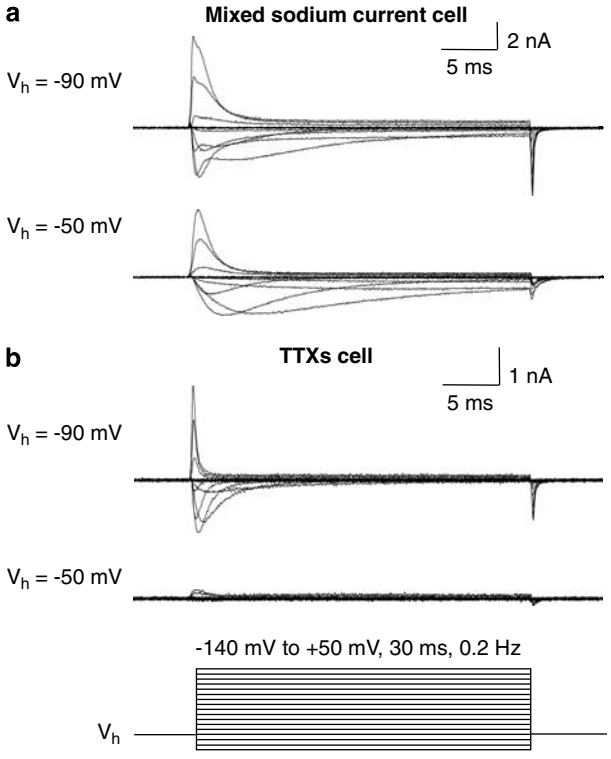

Figure 1 Isolation of TTXR current using a holding potential (V_h) of −50 mV. (**a**) Sodium current recorded from a cell containing both TTXS and TTXR sodium currents is shown. When this cell is held at a V_h of −50 mV, the faster TTXS component is inactivated leaving the isolated TTXR current. (**b**) Sodium current recorded in a cell that expressed purely TTX-sensitive (TTXS) currents is shown. When a V_h of −50 mV is used, no current is observed as, at this potential, the TTXS sodium channels have undergone voltage-dependent inactivation. The protocol used for all recordings is shown underneath.

intracellular solution in order to block calcium currents and facilitate identification of sodium current through $Na_V1.9$ channels, however we prefer not to use this method for the isolation of sodium currents. Fluoride only partially blocks calcium currents in sensory neurones (see e.g. Todorovic and Lingle, 1998), and can act to inhibit protein phosphatases, stimulate G proteins, increase the hydrophobicity of proteins and may modulate the biophysical properties of the $Na_V1.9$ channel. Therefore, our preference is to use chloride as our major intracellular anion. Reagents were purchased from either Sigma (UK) or VWR (Lutterworth, UK). In some experiments, $LaCl_3$ was omitted and/or the extracellular $CaCl_2$ concentration was reduced to 50 μM. Capacity transients were cancelled and series resistance was compensated by 70–80% (10 μs lag) by the 'feedback' method using the controls available on the amplifier (Cairn Optopatch or Axopatch 3). Background leak currents were subtracted using a P/8 protocol. Data were low-pass-filtered at 2–5 kHz, digitally sampled at 20–50 kHz and acquired using pClamp v7 or v8 software.

Drug treatments

Extracellular agents (TTX or La^{3+}) were applied either by addition to the superfusate (data in Figures 1–6) or through the use of a rapid application U-tube system (data in Figure 7). The rapid application system was employed to minimize the effect of current rundown, which tended to occur in experiments where the extracellular solution contained a low concentration of Ca^{2+}. Similar data, apart from speed of onset of effects, were obtained by either method of drug application.

As an example of this, we measured the relative increase in isolated TTXR sodium current amplitude 100 s after the application of TTX by the two methods. This time point was chosen as any increase in TTXR current as a result of TTX application had reached a plateau at this point. Addition via the superfusate produced an increase in isolated TTXR current amplitude of 43 ± 0.03%, and application by U-tube produced a slightly smaller increase of 32 ± 0.13%. These values were not significantly different when compared with a two-tailed Student's *t*-test. These data are taken from experiments shown in Figures 2b and 7a (La^{3+}, low Ca^{2+} data set).

Data analysis

Data were analysed using pClamp v8 (Axon Instruments, now Molecular Devices, Wokingham, UK) software and transferred to Excel (Microsoft, Washington, USA) spreadsheets for further statistical analysis.

Current–voltage relationships were produced by measuring the peak current amplitudes and plotting them against step voltage. The reversal potential was determined for each current by fitting a straight line of the equation $y = mx + c$ through the linear portion of the current–voltage relationship where the curve crosses the x axis, and calculating the value of x when $y = 0$. Currents from the current–voltage

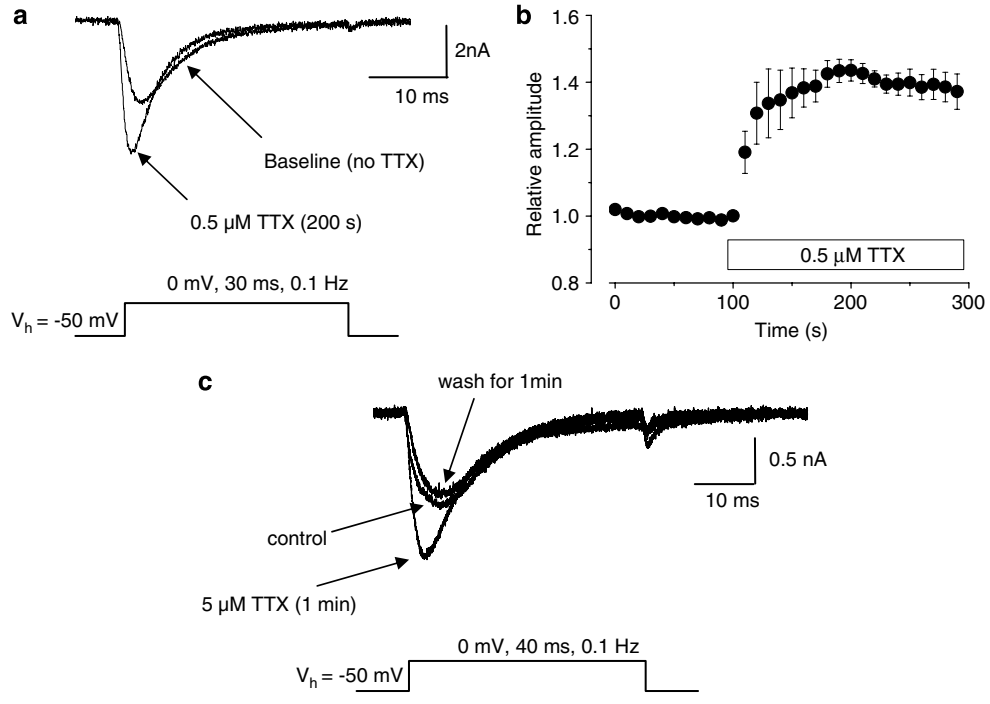

Figure 2 Application of 0.5 μM TTX increases TTXR current. (**a**) Example traces of isolated TTXR current recorded from a single cell from a holding potential of −50 mV are shown, with the protocol used shown underneath. The TTXR current recorded 200 s after the addition of 0.5 μM TTX to the extracellular superfusate is increased in amplitude. (**b**) The time course of the increase in TTXR current amplitude in the presence of TTX is shown. Current amplitudes are normalized to their baseline value ($n = 7$). (**c**) The enhancing effect of TTX on TTXR current is reversible. In this example, 5 μM TTX was applied to the cell, and this produced an increase in TTXR current amplitude. Following 1 min of washout in TTX-free buffer, the current returned to control levels.

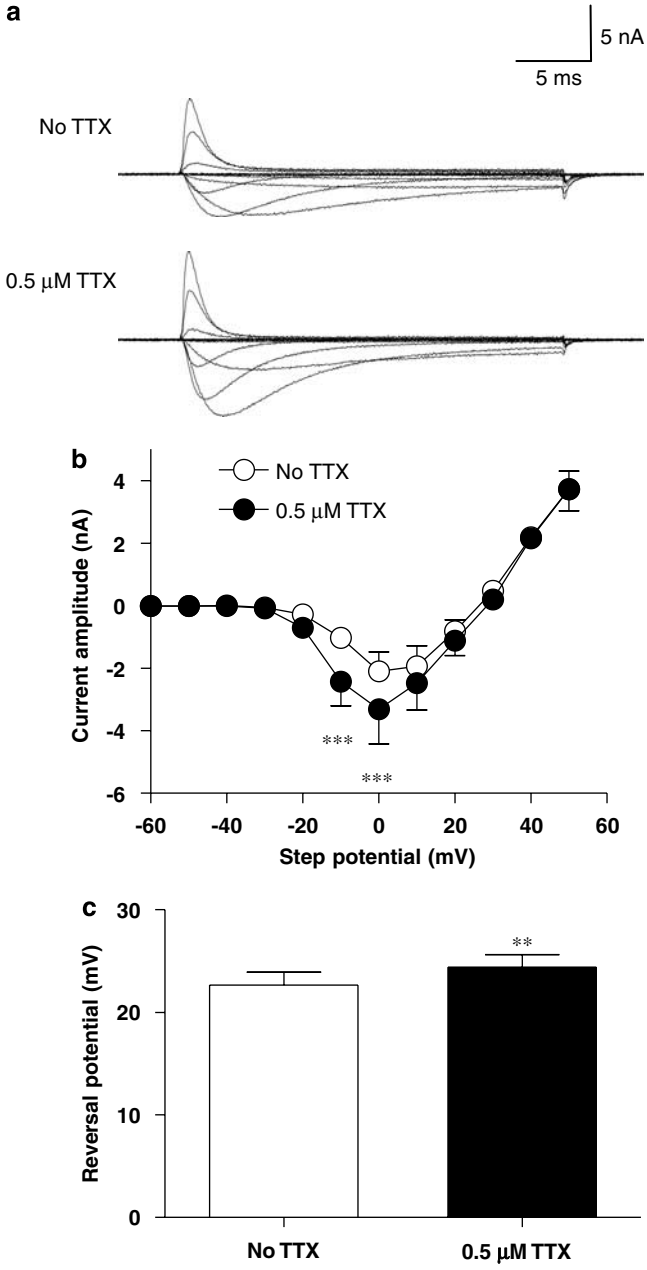

Figure 3 Effect of 0.5 μM TTX on the isolated TTXR current–voltage relationship. (**a**) Example recordings of isolated TTXR current–voltage protocols recorded from a single cell are shown. The top traces are in the absence of TTX and the lower traces in the presence of TTX. The application of TTX produces an increase in TTXR current amplitude. (**b**) The effect of 0.5 μM TTX on the average current–voltage relationship of the isolated TTXR current is shown. Data in the two groups are from the same cells ($n=7$) and are statistically compared using a repeated-measures two-way ANOVA with Bonferroni post-tests that reveals that at two step potentials, the increase in TTXR current produced by TTX is statistically significant (***$P<0.001$). Panel (**c**) shows that the average reversal potential of the isolated TTXR current is significantly increased in the presence of 0.5 μM TTX (**$P<0.01$, paired Student's *t*-test). Data are from the same cells as in panel b.

relationship were transformed into conductance values using the formula $G_{Na}=I/(V-V_{rev})$, where G_{Na} is the sodium conductance (S), I is the peak current (nA), V is the voltage step (mV) and V_{rev} is the reversal potential (mV). To create activation curves, conductance was normalized and average values were fitted with the following Boltzmann function: $G_{Na}/G_{Na}max=(A+(B-A))/(1+\exp((V_{50}-V)/k))$, where $G_{Na}/G_{Na}max$ is the normalized conductance value, A is the lowest value of the curve, B is the highest value of the curve, V_{50} is the voltage that produces half maximal conductance and k is the slope factor. To examine the rate of current activation, 10–90% rise times were determined from the beginning of the current response to the current peak. Data for the rates of development of inactivation of currents were fitted with single exponential functions as shown in Figure 5. Average asymptotes for the fits were -0.017 ± 0.03 nA before TTX application and -0.063 ± 0.03 nA in the presence of TTX.

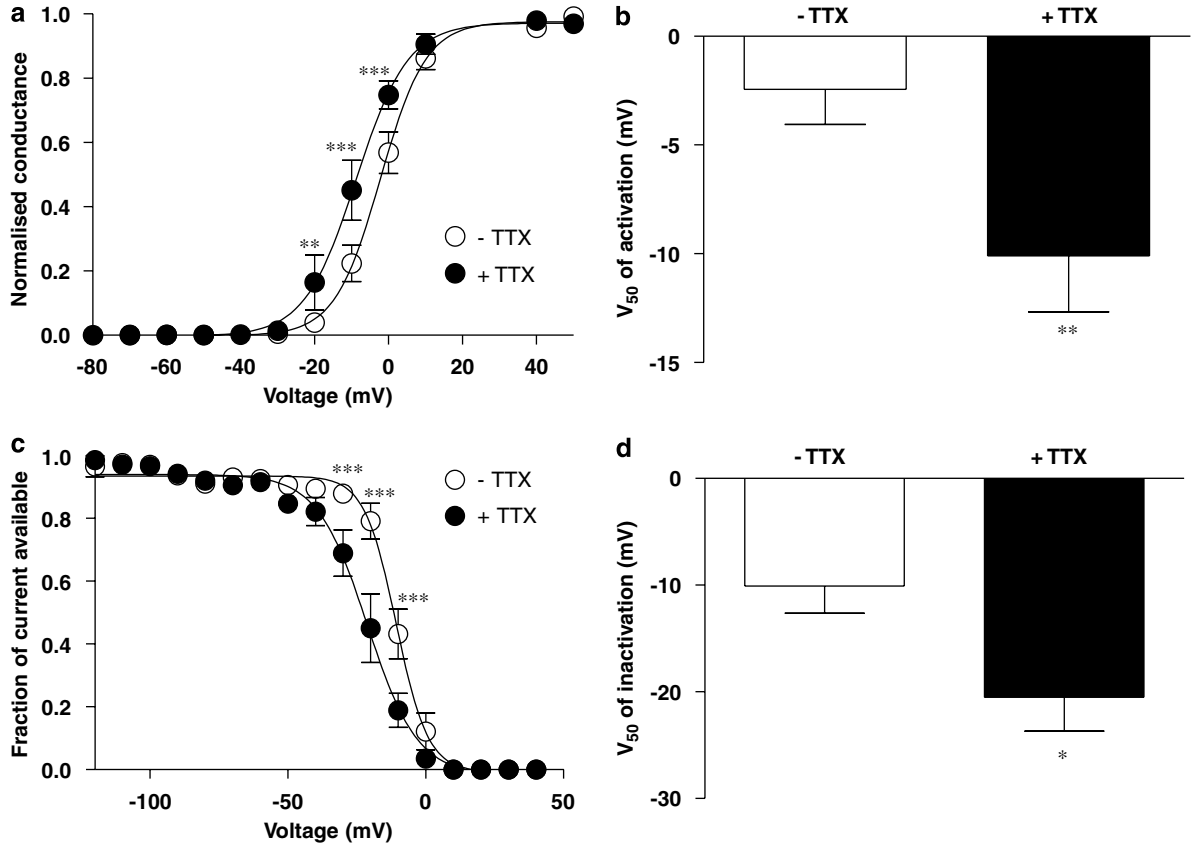

Figure 4 Effect of 0.5 μM TTX on voltage dependence of TTXR activation and fast inactivation. (**a**) Activation curves in the absence and presence of 0.5 μM TTX were created from the current–voltage relationship data shown in Figure 3. Addition of 0.5 μM TTX caused a negative shift in the activation curve. Significant differences between the two data sets are revealed by a two-way repeated-measures ANOVA with Bonferroni post-tests (**$P<0.01$, ***$P<0.001$). (**b**) The average V_{50} of activation for isolated TTXR currents in the presence of TTX is significantly more negative than in the absence of TTX (**$P<0.01$, paired Student's *t*-test). Data in both groups are recorded from the same cells ($n=7$). (**c**) Isolated TTXR current inactivation was assessed as described in the text. The inactivation curve for isolated TTXR currents is also shifted to the left by 0.5 μM TTX. A two way repeated-measures ANOVA with Bonferroni post-tests reveals significant differences between the two groups at three voltage steps (***$P<0.001$). (**d**) The average V_{50} of inactivation in the presence of 0.5 μM TTX is significantly more negative than in the absence of TTX, indicating a shift towards a more negative voltage dependence of fast inactivation (*$P<0.05$, paired Student's *t*-test). Data in both groups come from the same cells ($n=4$).

Curve fitting to graphical data was performed using Origin v4 (OriginLab, Northampton, MA, USA) or GraphPad Prism v4, and to current traces using pClamp v8. Dose–response data were fitted to a logistic equation as described previously (Docherty and Farrag, 2006). Unless otherwise stated, data are presented as mean ± s.e.mean. Statistical tests of differences between means were carried out by either paired, two-tailed Student's *t*-tests or repeated-measures two-way ANOVA, as indicated in the text. All channel and drug nomenclature in the text conform to that given in the BJP's Guide to Receptors and Channels (Alexander *et al*., 2007).

Results

Isolation of TTXR sodium current

To investigate the effects of TTX on TTXR currents in cells that express a mixture of both TTXR and TTXS VGSCs, the TTXR currents had to be isolated in the absence of TTX. Isolation was achieved by maintaining the cell at a holding potential of −50 mV, which is sufficiently positive to inactivate TTXS channels completely, while causing only a modest degree of inactivation of TTXR channels (Roy and Narahashi, 1992). An example of the TTXR current, that is, putative $Na_V1.8$, isolated by this method from a cell containing both TTXR and TTXS current components is shown in Figure 1a. Applying the same procedure to a cell containing purely TTXS sodium current reveals complete inactivation of TTXS currents at the more depolarized holding potential (Figure 1b). At a holding potential of −50 mV, any contribution of $Na_V1.9$ TTXR channels that might be present would be expected to be suppressed (Cummins *et al*., 1999), in which case the current evoked is predominantly $Na_V1.8$ TTXR current.

Effect of TTX on putative $Na_V1.8$ TTXR currents

Figure 2a shows an example of the effect of application of 0.5 μM TTX on a recording of putative $Na_V1.8$ current, and Figure 2b shows quantitative data from several similar experiments. Currents were evoked at a frequency of 0.1 Hz

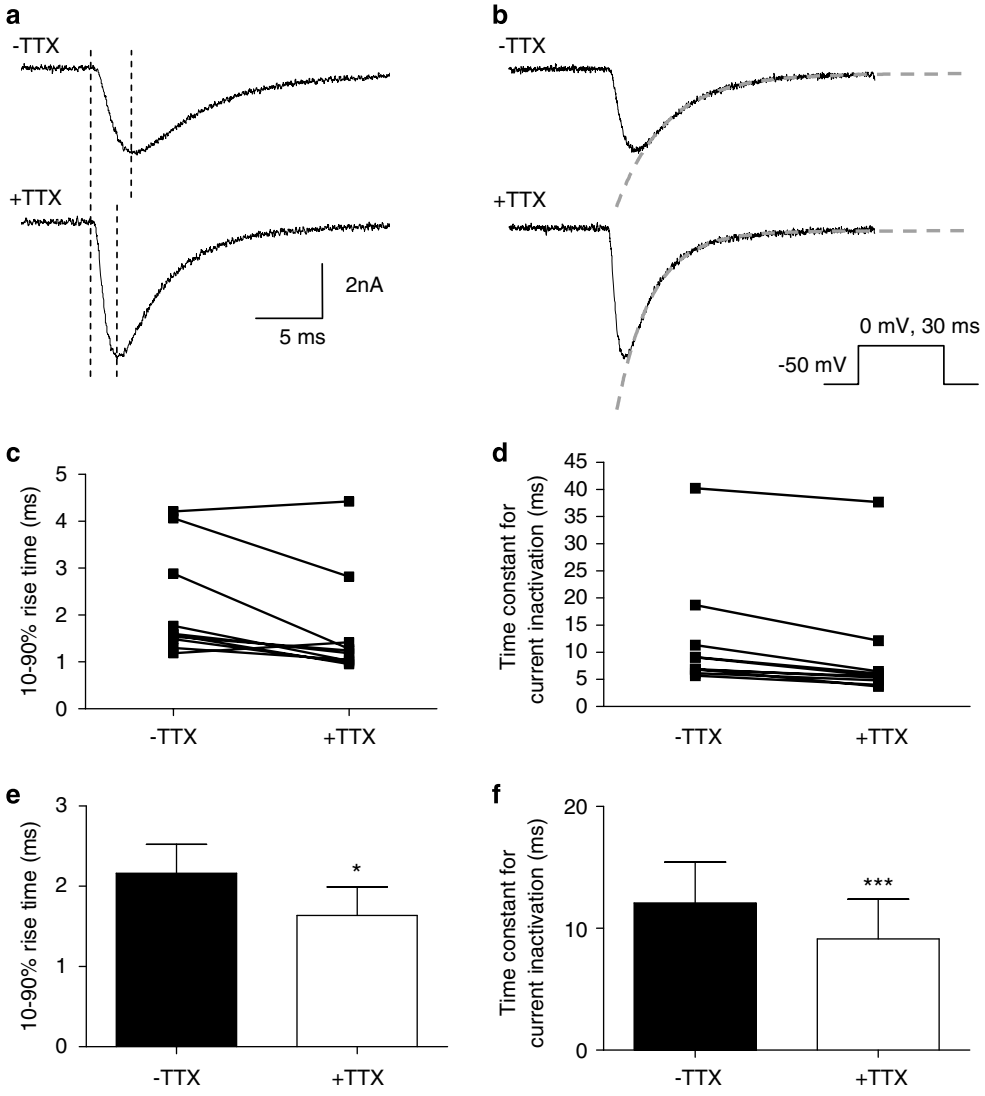

Figure 5 Effect of TTX on TTXR current kinetics. (**a** and **b**) The traces show examples of isolated TTXR current before (top trace) and after (bottom trace) application of TTX. The protocol used is shown. (**a**) Example of cursor placements (dashed lines) between which the 10–90% rise time of the current was measured to study the rate of current activation is shown. The dashed lines in panel b show how the exponential curves were fitted to study current inactivation rate. The fitted curve equations provide time constant measurements for the rate of inactivation. (**c** and **d**) The plots show individual cell data demonstrating how the 10–90% rise time (**c**) and rate of inactivation (**d**) are altered following the addition of 0.5 μM TTX. The averages and statistical comparisons of these data are shown in (**e**) and (**f**). (**e**) The average 10–90% rise time for TTXR current activation is reduced by the addition of 0.5 μM TTX, suggesting that the currents are activating faster (*$P<0.05$, paired Student's *t*-test). (**f**) The average time constant for TTXR current inactivation is significantly decreased in the presence of 0.5 μM TTX, suggesting that current inactivation is also faster (***$P<0.001$ paired Student's *t*-test). All data shown in panels **c** to **f** come from the same set of cells ($n=10$).

using a 30 ms step to the voltage which gave the maximum TTXR current amplitude (usually 0 mV) from a holding potential of –50 mV. The current amplitude increased when TTX was applied, and this increase was sustained in the continued presence of the drug. This effect of TTX was reversible as demonstrated by the recording in Figure 2c, where application of 5 μM TTX, the largest concentration used in all the experiments, caused an increase in TTXR current amplitude that returned to baseline levels following 1 min of washout with buffer.

Full current–voltage (I–V) curves were constructed in the absence and presence of TTX. The I–V protocol consisted of 30 ms voltage steps from a holding potential of −50 mV to a range of potentials between −140 and +50 mV every 5 s. The I−V curves showed that 0.5 μM TTX causes a significant increase in the amplitude of the current at activation potentials of −10 and 0 mV (Figures 3a and b). The measured reversal potential for the TTXR current was changed significantly (Figure 3c), but only by approximately 2 mV. Activation curves constructed from the I–V data (Figure 4a) showed that TTX causes a significant shift in the voltage that produces half-maximal activation (V_{50} for activation) by 7.7 ± 1.5 mV to more negative potentials (Figure 4b). To assess the voltage dependence of availability of TTXR current following channel inactivation, a protocol was used in which a 30 ms conditioning pre-pulse was applied to the cell immediately before a 30 ms test pulse to either 0 or −10 mV. The

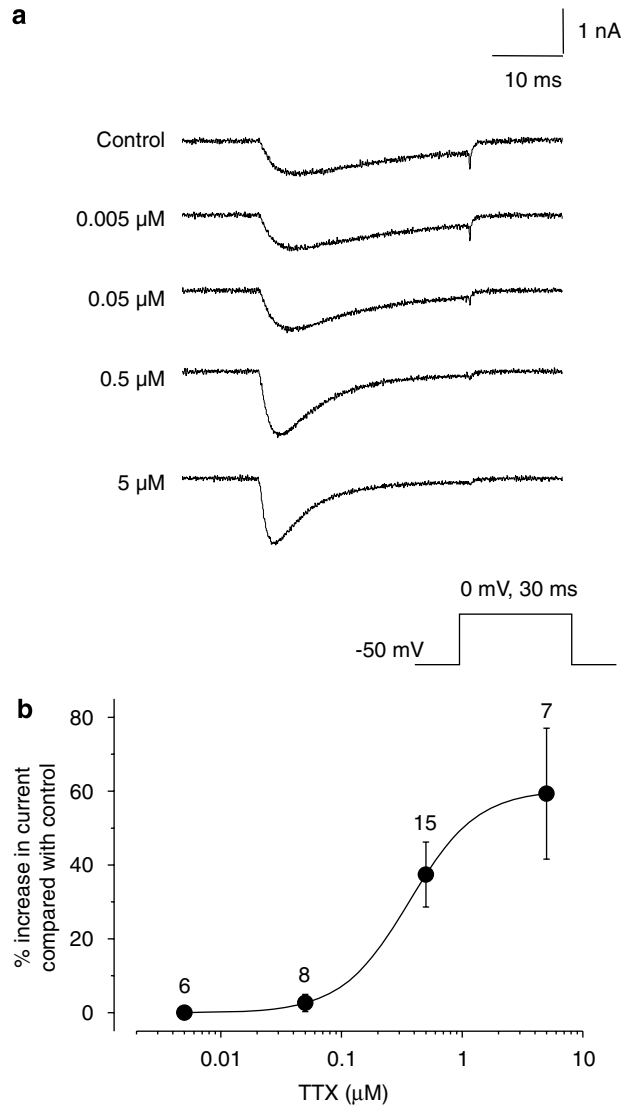

Figure 6 Dose–response of TTX on isolated TTXR currents. (**a**) Example traces of the isolated TTXR current response in a single cell exposed to different concentrations of TTX with the recording protocol shown below. (**b**) The dose–response curve for the effect of TTX was constructed as described in the methods. The lower concentrations of TTX had little effect on TTXR current size; however, a dose-dependent increase in TTXR current amplitude was seen at 0.5 and 5 μM TTX (*n* values are given above each data point).

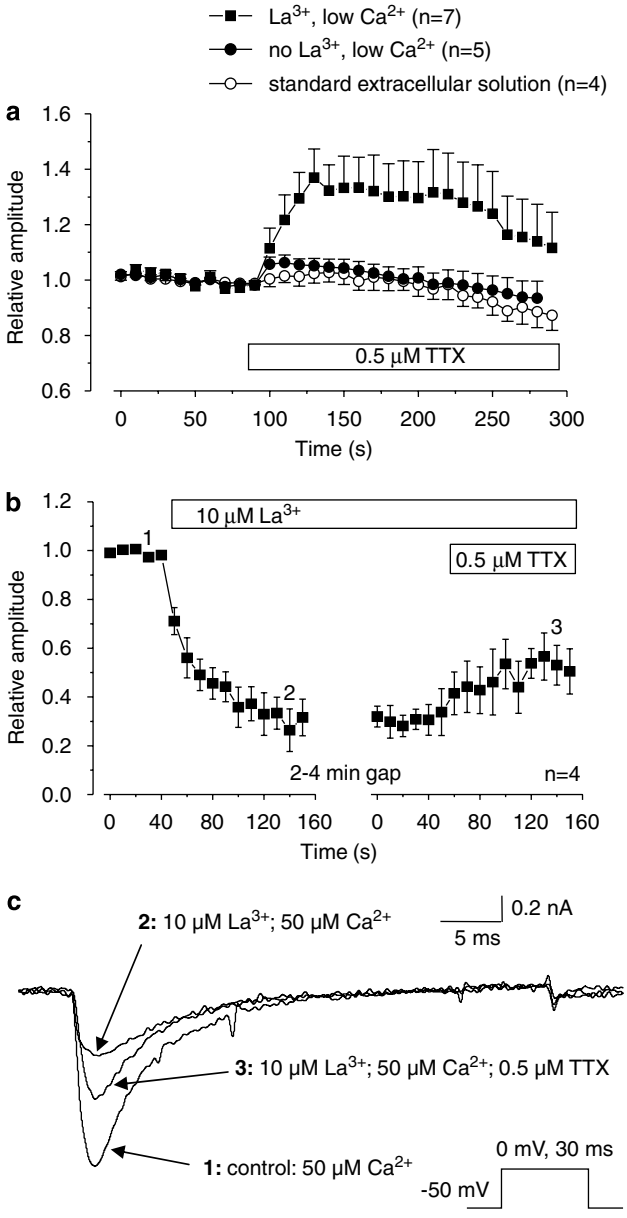

Figure 7 The involvement of extracellular La^{3+} in the enhancing effect of TTX on isolated TTXR currents. (**a**) The graph shows relative amplitudes of isolated TTXR current in modified extracellular solutions, with the bar showing the application of 0.5 μM TTX. TTXR currents were evoked as described in Figure 2. Reducing extracellular Ca^{2+} did not alter the enhancing effect of TTX on TTXR current. Reduction of Ca^{2+} plus removal of La^{3+} substantially reduced any current increase by TTX, suggesting that the effect is dependent on the presence of extracellular La^{3+}. In control experiments, recorded in standard extracellular solution, application of TTX-free extracellular solution to the cells had no effect on TTXR current amplitude. (**b**) The graph shows relative amplitudes of isolated TTXR current recorded in a low extracellular Ca^{2+} solution (50 μM) in the absence of extracellular La^{3+} and TTX. TTXR currents were evoked as described in Figure 2. The external application of 10 μM La^{3+} caused a sustained reduction in TTXR current amplitude of 60–70%. Subsequent addition of 0.5 μM TTX produced a partial reversal of this inhibition. The numbered data points on the graph correspond to the time points of the example traces shown in panel (**c**). (**c**) Example traces from data shown in panel b demonstrating the inhibition of TTXR current amplitude by 10μM La^{3+}, and the ability of 0.5 μM TTX to reverse this inhibition by La^{3+}.

conditioning pre-pulse was applied at a range of potentials and the resultant amplitude of current available in the test pulse was measured and plotted against pre-pulse potential (Figure 4c). As with channel activation, TTX also shifted the voltage dependence of inactivation to more negative potentials, with the V_{50} for inactivation being 10.4 ± 2.1 mV more negative in the presence of 0.5 μM TTX (Figure 4d).

The increase in TTXR current amplitude caused by TTX was associated with an acceleration of the rate of both current activation and current decay. The rate of activation was assessed by measuring the 10–90% rise time of the rising phase of each current before and after TTX application (Figure 5a). An analysis of the rate of inactivation of the current was performed by fitting single exponential

functions to the falling phase of the current as shown in Figure 5b. The plots in Figures 5c and d show how the 10–90% rise time (Figure 5c) and inactivation rate (Figure 5d) changes in individual cells following the extracellular application of TTX. The mean of these data and paired statistical comparisons are shown in Figures 5e and f. Comparing rates of activation and inactivation in the absence and presence of TTX showed that the 10–90% rise time of the current was significantly reduced by TTX (Figure 5e), and there was also a clear increase in the rate of inactivation after TTX application (Figure 5f).

Experiments were performed to test whether the effect of TTX on TTXR current amplitude was dose dependent. Figure 6a shows an example of a single DRG neurone where a range of concentrations of TTX from 5 nM to 5 μM were applied cumulatively to the same cell, and data showing averaged concentration response from several cells are shown in Figure 6b. The data show that the stimulating effect of TTX occurs at concentrations greater than 100 nM and predict an EC_{50} of 364 nM.

Effect of TTX on putative $Na_V1.9$ TTXR sodium current

In 15 recordings, the holding potential was changed to −120 mV to reveal putative $Na_V1.9$ TTXR currents, if they were present. This strategy also removed inactivation from TTXS currents so that the resulting current envelope provoked by a ladder of depolarizing voltage steps was complex and varied from cell to cell according to the complement of VGSCs in that cell, as previously reported by many others. Based mainly on the observations of Cummins *et al*. (1999), we used the simple criterion that any persistent current observed at the end of a 150 ms step to −50 mV from a holding potential of −120 mV was likely to be $Na_V1.9$ TTXR current. By this criterion, only one cell, of the 15 from which data were obtained using this protocol, expressed a putative $Na_V1.9$ TTXR current, and in that cell, 0.5 μM TTX caused a large increase in the size of the current, in much the same way as observed for putative $Na_V1.8$ TTXR (data not shown).

Involvement of extracellular polyvalent cations in the observed effect of TTX

Previously published work has shown that external polyvalent cations, including La^{3+}, can inhibit VGSC currents (Kuo *et al*., 2004) and also that external Ca^{2+} ions antagonize tonic binding of TTX to the closed state of VGSCs (Conti *et al*., 1996). The extracellular bathing solution used in the present experiments contained both Ca^{2+} at a concentration of 1 mM and 10 μM La^{3+}, the latter being used to block voltage-gated calcium channels and therefore prevent any contamination of the sodium current recordings by voltage-gated calcium currents. A possible explanation of the data would be that concentrations of TTX that are too low to block the channel nevertheless binds to and occupies the outer pore of the channel. The TTX may then prevent entry of Ca^{2+} or La^{3+} into the pore, thereby relieving a tonic blocking effect. To test this hypothesis, we repeated the experiment described in Figure 2 in an extracellular solution that did not contain La^{3+} and contained only 50 μM Ca^{2+}. This Ca^{2+} concentration was judged sufficient to maintain ionic selectivity of voltage-gated Ca^{2+} channels without contributing significant voltage-activated membrane current through them (Hess and Tsien, 1984). The enhancing effect of TTX was substantially reduced in the low Ca^{2+} solution in the absence of La^{3+} (Figure 7a). For comparison, and to evaluate the contribution of La^{3+} compared with Ca^{2+}, we repeated the experiment in a low Ca^{2+} solution, but with La^{3+} at the 10 μM concentration that is normally present in our extracellular bathing solution. Under these conditions, the enhancing effect of TTX was almost as large as that in the presence of normal extracellular Ca^{2+}, which suggests that the phenomenon is largely dependent on the presence of La^{3+} extracellularly (Figure 7a).

To further confirm the hypothesis that TTX was relieving a tonic block of the TTXR VGSC by extracellular La^{3+}, we carried out experiments to examine the effect of La^{3+} on the TTXR current. TTXR currents were recorded in the same low Ca^{2+} (50 μM) extracellular solution to suppress calcium currents, but in the absence of both TTX and La^{3+}. Addition of 10 μM La^{3+} to the extracellular solution caused a large reduction in TTXR current amplitude to around 35% of its original size (Figures 7b and c). Further application of 0.5 μM TTX to the extracellular solution produced a partial reversal of this blockade (Figures 7b and c). This confirms that 10 μM La^{3+} can indeed inhibit TTXR currents in DRG cells and supports our hypothesis that low concentrations of TTX can act to relieve this block.

Discussion and conclusions

Previous works in which authors have used TTX to block TTXS currents in DRG or trigeminal neurones to isolate TTXR sodium currents have not reported an enhancing effect of TTX on the residual TTXR current such as that described above, despite the presence of Ca^{2+} in extracellular solutions, as well as La^{3+} or another ionic blocker of voltage-gated calcium currents such as Cd^{2+}. There are at least two reasons that might account for this difference. Firstly, in the majority of studies where TTX has been used to block TTXS to isolate TTXR currents (including previous work from this laboratory), the TTX was applied to cells before recording and the development of the effect of TTX was not monitored routinely. Secondly, in studies where digital subtraction methods have been used to identify TTXS currents, TTX concentrations of 100 nM or less are frequently used (see e.g. Cummins and Waxman, 1997), and data presented here show that the enhancing effect of TTX on TTXR currents is barely measurable at such concentrations. However, the use of such low concentrations of TTX is not standard practice, and concentrations of TTX from 100 nM up to 1 μM are commonly used to block TTXS current.

This study shows that TTX causes a paradoxical increase in TTXR VGSC activity when Ca^{2+} and low concentrations of La^{3+} are present in the extracellular solution. Removal of La^{3+} from the extracellular solution greatly reduced the enhancing effect of TTX, which suggests that the effect is due, predominantly, to relief of a blocking action of La^{3+} on

TTXR VGSCs. In support of this, we have demonstrated that, at the relevant concentration of 10 μM, La^{3+} can block TTXR sodium currents in DRG neurones. Additionally, we have shown that application of TTX at a concentration that is too low to block the TTXR channel can partially reverse the inhibitory effect of La^{3+}.

The interpretation of our data is consistent with previous work that has shown that polyvalent cations inhibit VGSCs (Kuo *et al*., 2004) and also that they interfere with TTX binding (Conti *et al*., 1996). Here, we have demonstrated that the corollary is also true, that is, TTX interferes with the blocking action of polyvalent cations, even in TTXR VGSCs. Importantly, this effect occurs at surprisingly low concentrations, showing that TTX binds to TTXR sodium channels at a submicromolar concentration of the order of 100-fold less than the concentration that is required to block the channels. The present experiments have focussed on sodium currents carried through putative $Na_V1.8$ VGSCs, since, in our experience, these currents are more widely expressed in sensory neurones and are easier to record, but, in the single example of putative $Na_V1.9$ sodium current that we tested, the data were qualitatively similar, suggesting that both the major subtypes of TTXR VGSCs in rat sensory neurones are capable of binding TTX at submicromolar concentrations.

The TTX binding site of the VGSC is associated with the extracellular aspect of the pore region of the channel, and it has been studied previously in detail (Terlau *et al*., 1991; Penzotti *et al*., 1998; Choudhary *et al*., 2003). The binding site comprises a ring of four amino acids (EEDD) in the outer vestibule of the sodium channel pore, and an inner ring, also of four amino acids (DEKA), that creates the channel selectivity filter. The interaction of TTX with VGSCs is thought to be a sequential two-step process whereby the hydroxyl functions on the rigid molecular structure of TTX interact with the acidic residues of the outer ring, and then the positively charged guanidinium interacts with the DEKA group of the inner ring to block the channel (Penzotti *et al*., 1998). All of the key residues that are necessary for binding of TTX are present in all of the VGSC isoforms, including $Na_V1.8$ and $Na_V1.9$ isoforms. In the TTXR VGSCs, resistance to block by TTX seems to be conferred by a single residue that is adjacent to the conserved aspartate of the DEKA motif. In TTXR channels, the position is occupied by either a cysteine ($Na_V1.5$) or serine ($Na_V1.8$, 1.9), but in TTXS channels, it is occupied by a more lipophilic residue, either tyrosine ($Na_V1.3$, 1.4, 1.6 and 1.7) or phenylalanine ($Na_V1.1$, 1.2). In the absence of a lipophilic residue, in this position, the positively charged guanidinium 'head' of the TTX molecule cannot engage with the DEKA residues to produce a block of the channel. Our data demonstrate clearly that low concentrations of TTX increase the size of TTXR sodium currents. Thus, although the charged guanidinium head of the molecule cannot block the channels, the TTX molecule must nevertheless bind to the channel.

As the guanidinium group of TTX is positively charged, binding near the external mouth of the channel would be expected to cause a positive shift in the activation potential, if anything. Such a positive shift has been reported to be previously associated with the effect of Ca^{2+} ions on the channels (Boccaccio *et al*., 1998). The enhancing effect of TTX was associated with a negative shift of the V_{50} for activation of $Na_V1.8$ of about 8 mV. This shift would be explained if TTX, when bound, prevents access of La^{3+} to a binding site in the channel so that there is a net reduction in positive charge density. Polyvalent cations including La^{3+} have been shown previously to block both putative $Na_V1.8$ (Kuo *et al*., 2004) and $Na_V1.9$ (Coste *et al*., 2007) sodium currents. The acceleration of the kinetics of fast inactivation and activation that we observed is also consistent with relief of polyvalent ion block, because La^{3+} has been shown previously to cause a slowing of both inactivation and activation kinetics associated with its blocking action, although at the slightly higher concentration of >30 μM (Kuo *et al*., 2004).

At 10 μM La^{3+}, Kuo *et al* (2004) report an approximate 15% reduction in TTXR current amplitude, whereas we observed a much greater decrease in current amplitude (60–70%). The reasons for this quantitative difference are unclear, but it could reflect other methodological differences between the two studies. The results of our study also revealed that TTX caused a significant shift in TTXR current reversal potential, but the small magnitude of the observed change (less than 2 mV) would suggest that this is unlikely to be an important feature of the actions of La^{3+}, or one of great consequence.

The enhancing effect of TTX on current amplitude was only slightly reduced in 50 μM extracellular Ca^{2+} when La^{3+} was still present, so it is likely that relief of channel block by La^{3+}, rather than Ca^{2+}, provides the main contribution to the phenomenon. It is possible that relief of La^{3+} blockade by TTX might help to counteract the effects of La^{3+} on channel gating in those experiments in which both TTX and La^{3+} are present in the extracellular medium.

The pharmacology of TTXR VGSCs is difficult to explore using methods other than voltage-clamp electrophysiological approaches in single cells. Heterologous expression of the $Na_V1.8$ and $Na_V1.9$ channels has been achieved, but is difficult compared with most TTXS VGSC subtypes. To study TTXR in the native system of the sensory neurone, TTXR channels must be isolated from TTXS and this is usually achieved by adding low concentrations of TTX to the extracellular bathing medium. Whatever the mechanism of the effect, the data presented above show that TTX binds to TTXR sodium channels at low concentrations even though it does not block the channel. Importantly, it follows that TTX will compromise the pharmacological evaluation of potential channel-blocking agents that interact with the channel pore, and this includes most known VGSC blockers. The same considerations are likely to be true for La^{3+} and perhaps for other polyvalent ions that are included to block voltage-gated calcium channels, such as Cd^{2+}. So far as we are aware, this is the first demonstration of a clear distinction between the binding affinity of a channel-blocking agent and its potency in blocking the channel. These observations should be taken into consideration when designing assay systems for the evaluation of drugs that block TTXR VGSCs.

Acknowledgements

We acknowledge financial support from the Medical Research Council, the Multiple Sclerosis Society of Great Britain and Northern Ireland and the European Union (NeuroproMiSe).

Conflict of interest

The authors state no conflict of interest.

References

Akopian AN, Sivilotti L, Wood JN (1996). A tetrodotoxin-resistant voltage-gated sodium channel expressed by sensory neurons. *Nature* **379**: 257–262.

Akopian AN, Souslova V, England S, Okuse K, Ogata N, Ure J *et al*. (1999). The tetrodotoxin-resistant sodium channel SNS has a specialized function in pain pathways. *Nat Neurosci* **2**: 541–548.

Alexander SPH, Mathie A, Peters JA (2007). Guide to Receptors and Channels (GRAC), 2nd edition (2007 revision). *Br J Pharmacol* **150** (Suppl. 1): S1–S168.

Arbuckle JB, Docherty RJ (1995). Expression of tetrodotoxin-resistant sodium channels in capsaicin-sensitive dorsal root ganglion neurons of adult rats. *Neurosci Lett* **185**: 70–73.

Boccaccio A, Moran O, Conti F (1998). Calcium dependent shifts of Na^+ channel activation correlated with the state dependence of calcium-binding to the pore. *Eur Biophys J* **27**: 558–566.

Cestèle S, Catterall WA (2000). Molecular mechanisms of neurotoxin action on voltage-gated sodium channels. *Biochimie* **82**: 883–892.

Choudhary G, Yotsu-Yamashita M, Shang L, Yasumoto T, Dudley Jr SC (2003). Interactions of the C-11 hydroxyl of tetrodotoxin with the sodium channel outer vestibule. *Biophys J* **84**: 287–294.

Conti F, Gheri A, Pusch M, Moran O (1996). Use dependence of tetrodotoxin block of sodium channels: a revival of the trapped-ion mechanism. *Biophys J* **71**: 1295–1312.

Coste B, Crest M, Delmas P (2007). Pharmacological dissection and distribution of NaN/Nav1.9, T-type Ca2+ currents, and mechanically activated cation currents in different populations of DRG neurons. *J Gen Physiol* **129**: 57–77.

Cummins TR, Dib-Hajj SD, Black JA, Akopian AN, Wood JN, Waxman SG (1999). A novel persistent tetrodotoxin-resistant sodium current in SNS-null and wild-type small primary sensory neurons. *J Neurosci* **19**: RC43(1–6).

Cummins TR, Waxman SG (1997). Downregulation of tetrodotoxin-resistant sodium currents and upregulation of a rapidly repriming tetrodotoxin-sensitive sodium current in small spinal sensory neurons after nerve injury. *J Neurosci* **17**: 3503–3514.

Docherty RJ, Farrag KJ (2006). The effect of dibutyryl cAMP on tetrodotoxin-sensitive and -resistant voltage-gated sodium currents in rat dorsal root ganglion neurons and the consequences for their sensitivity to lidocaine. *Neuropharmacology* **51**: 1047–1057.

Dib-Hajj S, Black JA, Cummins TR, Waxman SG (2002). NaN/Nav1.9: a sodium channel with unique properties. *Trends Neurosci* **25**: 253–259.

Elliott AA, Elliott JR (1993). Characterization of TTX-sensitive and TTX-resistant sodium currents in small cells from adult rat dorsal root ganglia. *J Physiol* **463**: 39–56.

Hess P, Tsien RW (1984). Mechanism of ion permeation through calcium channels. *Nature* **309**: 453–456.

Kostyuk PG, Veselovsky NS, Tsyndrenko AY (1981). Ionic currents in the somatic membrane of rat dorsal root ganglion neurons—I. *Sodium Curr Neurosci* **6**: 2423–2430.

Kuo CC, Chen WY, Yang YC (2004). Block of tetrodotoxin-resistant Na^+ channel pore by multivalent cations: gating modification and Na^+ flow dependence. *J Gen Physiol* **124**: 27–42.

Lai J, Porreca F, Hunter JC, Gold MS (2004). Voltage-gated sodium channels and hyperalgesia. *Annu Rev Pharmacol Toxicol* **44**: 371–397.

McLean MJ, Bennett PB, Thomas RM (1988). Subtypes of dorsal root ganglion neurons based on different inward currents as measured by whole-cell voltage clamp. *Mol Cell Biochem* **80**: 95–107.

Narahashi T (1974). Chemicals as tools in the study of excitable membranes. *Physiol Rev* **54**: 813–889.

Pearce RJ, Duchen MR (1994). Differential expression of membrane currents in dissociated mouse primary sensory neurons. *Neuroscience* **63**: 1041–1056.

Penzotti JL, Fozzard HA, Lipkind GM, Dudley Jr SC (1998). Differences in saxitoxin and tetrodotoxin binding revealed by mutagenesis of the Na^+ channel outer vestibule. *Biophys J* **75**: 2647–2657.

Renganathan M, Dib-Hajj S, Waxman SG (2002). Na(v)1.5 underlies the 'third TTX-R sodium current' in rat small DRG neurons. *Mol Brain Res* **106**: 70–82.

Roy ML, Narahashi T (1992). Diferential properties of tetrodotoxin-sensitive and tetrodotoxin-resistant sodium channels in rat dorsal root ganglion neurons. *J Neurosci* **12**: 2104–2111.

Rush AM, Bräu ME, Elliott AA, Elliott JR (1998). Electrophysiological properties of sodium current subtypes in small cells from adult rat dorsal root ganglia. *J Physiol* **511**: 771–789.

Rush AM, Cummins TR, Waxman SG (2007). Multiple sodium channels and their roles in electrogenesis within dorsal root ganglion neurons. *J Physiol* **579**: 1–14.

Sangameswaran L, Delgado SG, Fish LM, Koch BD, Jakeman LB, Stewart GR *et al*. (1996). Structure and function of a novel voltage-gated, tetrodotoxin-resistant sodium channel specific to sensory neurons. *J Biol Chem* **271**: 5953–5956.

Terlau H, Heinemann SH, Stühmer W, Pusch M, Conti F, Imoto K *et al*. (1991). Mapping the site of block by tetrodotoxin and saxitoxin of sodium channel II. *FEBS Lett* **293**: 93–96.

Todorovic SM, Lingle CJ (1998). Pharmacological properties of t-type Ca^{2+} current in adult rat sensory neurons. *J Neurophysiol* **79**: 240–252.